

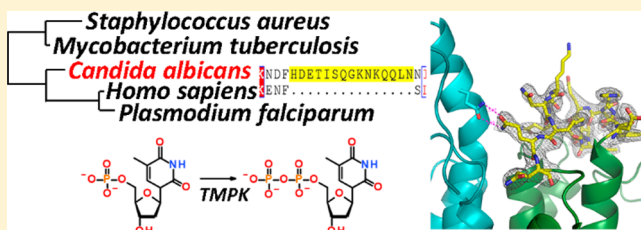
The Structure of Thymidylate Kinase from *Candida albicans* Reveals a Unique Structural Element

Kaustubh Sinha and Gordon S. Rule*¹

Department of Biological Sciences, Carnegie Mellon University, Pittsburgh, Pennsylvania 15213, United States

S Supporting Information

ABSTRACT: The structure of thymidylate kinase from *Candida albicans*, determined by X-ray crystallography, is reported to a resolution of 2.45 Å with a final R_{free} of 0.223. Thymidylate kinase from *C. albicans* possesses a unique 15-residue loop that is not seen in thymidylate kinases from other genera. The structure reported here reveals that the conformation of this loop is constrained by both intra- and intersubunit hydrogen bonding, and a number of key residues in this loop are conserved among different *Candida* species that are medically important. The substrate specificity of the enzyme was determined using a novel nuclear magnetic resonance-based assay as well as a traditional coupled assay. The enzyme is active against 3'-azido-3'-deoxythymidine monophosphate and moderately active with dGMP. The distinct functional and structural differences between the *C. albicans* enzyme and the human enzyme suggest that thymidylate kinase is an appropriate target for the development of new antifungal agents.



Thymidylate kinases (TMPKs, EC 2.7.4.9) use ATP to phosphorylate TMP to TDP in the presence of a divalent cation, typically Mg^{2+} .¹ TMPKs from different species show significant structural homology despite a low degree of sequence similarity. For example, although the degree of sequence similarity between the human and *Plasmodium falciparum* TMPK is only 52%, their structures align with a root-mean-square deviation (RMSD) of 0.96 Å for the main-chain atoms. All TMPKs appear to be homodimers, and each monomer consists of a five-stranded β -sheet surrounded by 7–11 α -helices (Figure 1). The active site of TMPKs can be divided into two important regions that are required for catalysis: the ligand-induced degradation (LID) region and the P-loop. The LID is a flexible region of the protein that closes on the active site and allows the transfer of the phosphate group from ATP to TMP. The P-loop is involved in binding and positioning the α - and β -phosphoryl groups of ATP. This region of the protein shifts from a relatively open form in the presence of ADP and TMP to a closed form when the product analogue Ap_3T is bound. In particular, residue Asp 15 within the P-loop swings into the active site in the closed form and forms a hydrogen bond with the 3'-OH of TMP.²

Type I TMPKs, which include the TMPKs from human (hTMPK) and *Saccharomyces cerevisiae* (γ TMPK), possess conserved Arg and Asp residues in the P-loop that are critical for catalysis. On the other hand, type II TMPKs, such as that from *Escherichia coli*, do not have a conserved basic residue in the P-loop but instead have one or more basic residues in the LID region that aid in catalysis (see Figure 2 for representative sequences for type I TMPKs).

Because TMPK lies at the intersection of the de novo (mediated by thymidylate synthase) and salvage (mediated by thymidine kinase) pathways for thymidine synthesis,¹ it is an

essential enzyme for the production of thymidine triphosphate. The expression of TMPKs is regulated by the cell cycle to provide the high levels of thymidine that are required for DNA replication.^{6,7} TMPK is also required for DNA repair processes in tumor cells, and the inhibition of TMPK levels in combination with doxorubicin, which induces DNA repair, is lethal to colon cancer cells.⁸ In the case of LKB1-based lung cancers, direct inhibition of thymidylate kinase activity has been shown to be lethal.⁹ Consequently, inhibitors of human TMPK are potential anticancer agents.

Human TMPK is involved in the activation of thymidine analogue prodrugs such as 3'-azido-3'-deoxythymidine (AZT or Zidovudine), which is a potent retroviral drug used in the treatment of HIV infection.¹⁰ The active form of AZT is the triphosphate (AZTTP), which is an alternate substrate to TTP for HIV reverse transcriptase, leading to chain termination because of the missing 3'-OH group in AZT. Because TMPK is responsible for the addition of the second phosphate group to AZT, it is an essential component of the AZT activation pathway. The inefficient conversion of AZTTP to AZTDP by the human enzyme¹¹ is the principal reason for the toxicity of AZT,¹² limiting its current use mainly to perinatal treatment to protect newborns delivered from HIV-infected mothers (<http://aidsinfo.nih.gov/guidelines>). The toxicity of AZT has been exploited as a suicide enzyme in gene therapy.¹³ In this case, human TMPK has been engineered for high catalytic activity against AZTTP¹¹ and the gene for the catalytically enhanced enzyme has been inserted into vectors for gene

Received: May 23, 2017

Revised: July 24, 2017

Published: July 25, 2017

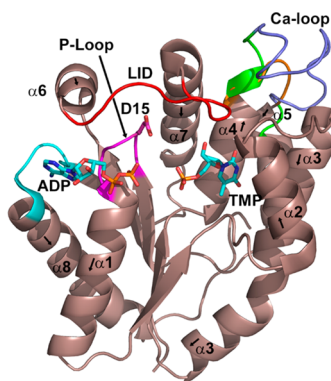


Figure 1. Structure of human TMPK and the location of the Ca-loop in *Candida albicans* TMPK. The complete structure of a single monomer of dimeric human TMPK is shown (PDB entry 1E2D²), along with the additional loop found in the *C. albicans* enzyme (Ca-loop), which was determined in this study. The additional loop in the *C. albicans* enzyme is colored slate blue, with adjacent regions colored green. The corresponding loop in the human enzyme is colored orange. The remainder of the human enzyme is colored dark salmon, except for the P-loop region (magenta), the LID region (red), and the ADP binding region (cyan). The location of Asp15 in the P-loop is indicated (D15). Bound ADP and TMP are rendered as sticks, with carbons colored cyan. The helices are labeled (numbering as in Figure 2); the arrow indicates the direction of the helix (N → C). Note that helix 3 is labeled at both its N- and C-terminal ends. Figure generated using Pymol.³

therapy. In addition to activation of AZT by the human enzyme, a number of other antiviral prodrugs are activated by viral thymidylate kinases.¹⁴

The crucial role of thymidine in DNA replication has made TMPKs attractive drug targets for the development of antibiotics for the treatment of infectious diseases. Several inhibitors have been developed against TMPKs from many pathogenic bacterial and protozoan species, including *Mycobacterium tuberculosis* and *P. falciparum*.^{15–19} Selective inhibition of TMPK is possible because of significant sequence differences between human and pathogen forms of TMPK, as

illustrated by a phylogenetic analysis (Figure 3A). Sequence differences also translate to differences in biochemical properties. For example, the enzyme from *P. falciparum* is capable of using either TMP or dGMP as a substrate at similar rates,²⁰ and this enzyme, along with the enzyme from *E. coli*,²¹ is also proficient at phosphorylating AZTMP. In contrast, as discussed above, the human enzyme is not proficient at using AZTMP as a substrate²² and does not bind dGMP.^{23,24}

Efforts thus far have been focused on developing TMPK inhibitors for the treatment of bacterial and protozoal infections; inhibitors with antifungal properties have not been actively pursued. The fungal pathogen *C. albicans* is responsible for the majority of medically related fungal infections because of its ability to form biofilms on catheter lines and other implants.²⁵ Additional *Candida* species, such as *Candida dubliniensis*, cause fungal infections in immunocompromised individuals,²⁶ and *Candida tropicalis* is a common fungal pathogen in tropical areas.²⁷ *Candida* infections are especially dangerous in patients with impaired immunity, such as those suffering from AIDS or undergoing cancer therapy. Fluconazole is the first line of treatment for localized and systemic *C. albicans* infections.²⁸ However, long-term use of fluconazole in immunocompromised patients results in the emergence of drug resistant strains, some of which are resistant to wider spectrum antifungals.²⁹ There is thus a need to identify new drug targets to combat *Candida* infections.

An important first step toward the development of TMPK-based antifungal agents is to determine the differences in the biochemical and structural properties of TMPK from *C. albicans* (CaTMPK) versus the human enzyme. The aligned amino acid sequences of CaTMPK, γ TMPK, and hTMPK are shown in Figure 2. Although the P-loop (GXXXXGK) at the N-terminus, the LID region at residue 160, and the dimer interface (helix α 3) are well-conserved, a unique aspect of the CaTMPK sequence is the presence of 15 additional residues between helices α 4 and α 5 (termed the Ca-loop). This interhelical loop in the human and *S. cerevisiae* enzymes is much smaller (6–8 residues long). These additional residues appear to be unique to *Candida* species except for *Candida glabrata*,

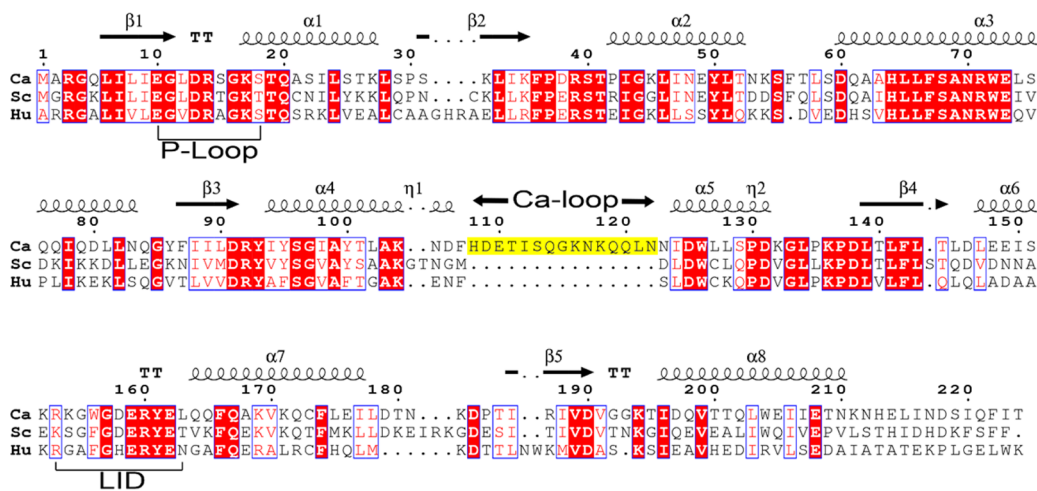


Figure 2. Alignment of sequences for TMPKs from *C. albicans* (Ca), *S. cerevisiae* (Sc), and human (Hu). Sequence alignment obtained using MUSCLE⁴ and displayed using ESPrnt 3.0.⁵ The additional 15 residues in the loop between α 4 and α 5 that are unique to the *C. albicans* enzyme are highlighted in yellow. This segment is termed the Ca-loop. The secondary structure is based on the *C. albicans* enzyme structure reported here. The long third helix in the *C. albicans* enzyme is usually considered to be broken into two separate helices in the human enzyme. UniProt codes are C4YCM5, P00572, and P23919 for the *C. albicans*, *S. cerevisiae*, and human enzymes, respectively.

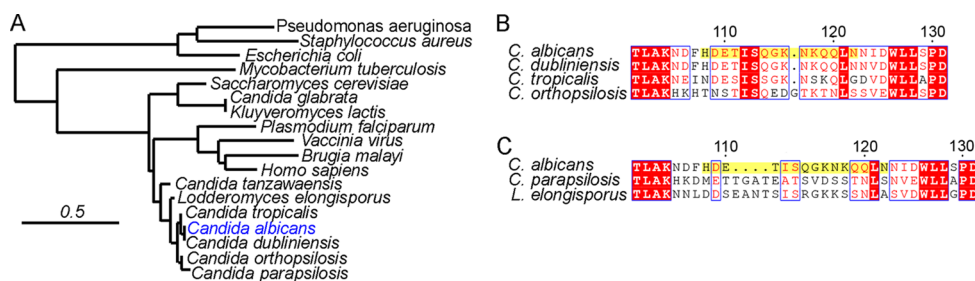


Figure 3. Phylogenetic tree of TMPK sequences and alignment of the loop region in *C. albicans* with related species. Panel A shows a phylogenetic tree generated using Phylogeny.fr³⁰ for selected TMPKs. TMPK from *C. albicans* is distantly related to human TMPK but closely related to those of other *Candida* species. Panels B and C show the Ca-loop region of caTMPK (Ca-loop is highlighted in yellow) aligned with TMPKs from species related to *C. albicans*. Panel B shows that the length of the loop and key residues I112, S113, and L121 are highly conserved in *C. albicans*, *C. dubliniensis*, *C. tropicalis*, and *Candida orthopsilosis*. K118 is also conserved in these four TMPKs, except shifted by a residue in *C. tropicalis*, becoming K119. Panel C shows that the Ca-loop is elongated by four residues in *Candida parapsilosis* and *Lodderomyces elongisporus*, with a lower degree of sequence conservation.

which is distant from other *Candida* species and more similar to *Kluyveromyces lactis* and *S. cerevisiae* (see Figure 3A). Sequence alignment of TMPKs from various species closely related to *C. albicans* shows that this loop, or a longer variant, is common and contains a number of conserved residues (Figure 3B,C). The additional residues that are found in these *Candida* species may confer unique structural and functional features that could be exploited for drug development. Other organisms, such as *Ehrlichia chaffeensis* and *Sulfolobus tokodaii*, have insertions elsewhere in the enzyme (see Figure S7), and the role of these insertions is currently unknown.

Because the additional residues in the *C. albicans* TMPK are absent in TMPKs of known structure, it is difficult to predict if this region is structured and could serve as potential drug binding sites that would be unique to *C. albicans*. Here we report the first structure of TMPK from *C. albicans* and show that the additional residues do not alter the overall structure of the enzyme; however, the loop formed by the inserted residues is well structured by several intra- and intersubunit interactions.

We also introduce a new simple one-step nuclear magnetic resonance (NMR) assay to measure the addition of a phosphate group to TMP, dGMP, or AZTMP by kinases. The assay allows for the near-continuous monitoring of the reaction and is useful in screening for inhibitors because it does not suffer some of the complications associated with other methods, such as interference of the coupling enzymes by compounds in a library of potential inhibitors.³¹ The structural and biochemical differences between human and *C. albicans* TMPK reported here suggest that it should be possible to develop specific TMPK inhibitors against this fungal pathogen, as well as other pathogenic *Candida* species.

METHODS

Protein Expression and Purification. The thymidylate kinase encoded by the CDC8 gene of *C. albicans* has not been purified or characterized previously. A synthetic gene codon-optimized for expression in *E. coli* was obtained from DNA 2.0 and cloned into the pet22b(+) vector using the NdeI and XhoI sites on the plasmid. The N-terminus of the expressed protein has the sequence MHHHHHNYFYQGSTSARG, consisting of a (His)₆ tag followed by a TEV protease site (ENLYFQG). After cleavage with TEV protease, the amino-terminal sequence is GSTSARG. The sequence of the native protein begins with MARG. To maintain consistency with the numbering of residues in the native protein, the residues in our TEV-treated

protein are numbered as G(-2)S(-1)T(0)S(1)A(2)R(3)G(4), etc. Gly(-2) and Ser(-1) are not observed in the electron density map. The protein was expressed in C3013 T7 Express lysY/Iq *E. coli* cells from New England Biolabs.

The cells were grown in Luria-Bertani (LB) medium containing 100 mg/mL ampicillin at 30 °C to an A₆₀₀ of 0.8 and induced with 1 mM isopropyl β-D-thiogalactoside (IPTG) for 4 h. After being harvested, the cells were stored at -80 °C. The cell pellets were resuspended in buffer A [50 mM sodium phosphate, 300 mM sodium chloride, 10 mM imidazole, and 50 μM TMP (pH 7.4)] and lysed by sonication. The lysate was centrifuged at 20000g for 40 min at 4 °C. An appropriate amount of HisPur Cobalt Resin (Thermo Scientific) was then added to the supernatant and mixed on an end-over-end rotator for 1 h. This supernatant/resin mix was then poured into a gravity chromatography column to separate the resin from the flow-through. The resin was then washed with 3 column volumes of buffer A. The protein was then eluted with buffer B [50 mM sodium phosphate, 300 mM sodium chloride, and 150 mM imidazole (pH 7.4)] and then dialyzed against the TEV cleavage buffer [50 mM Tris-HCl, 0.5 mM EDTA, and 1 mM DTT (pH 8.0)]. TEV protease was then added to the protein and incubated at 4 °C to allow for overnight digestion. The reaction mix was then dialyzed against buffer A (without TMP) to remove DTT and EDTA. The digested sample was then allowed to flow through a HisPur Cobalt Resin gravity column and washed with buffer A. The flow through containing the CaTMPK with the His tag cleaved was collected and dialyzed against buffer C [50 mM potassium phosphate, 50 mM NaCl, 1 mM EDTA, and 1 mM DTT (pH 8.0)]. The sample was then loaded on a Q-Sepharose Fast Flow (GE Healthcare) column equilibrated with buffer C. The protein was eluted using a salt gradient (buffer C, from 0.05 to 1.5 M NaCl), concentrated, and passed through a gel filtration column [Sephadex G-75; 20 mM HEPES, 50 mM NaCl, 1 mM EDTA, and 1 mM DTT (pH 7.5)]. The purified protein was concentrated to 10 mg/mL and stored at 4 °C. Typically, the yield was 70 mg of protein from 1 L of bacterial culture.

Crystallization and Data Collection. The complex of CaTMPK with 1 mM ADP, 1 mM TMP, and 10 mM Mg²⁺ was used to set up crystal trials. Initial screens were performed using precipitants that also acted as cryo-protective agents (see ref 32). Diffraction quality crystals were obtained by mixing 3 μL of the CaTMPK-ADP-TMP-Mg²⁺ complex with 3 μL of the reservoir solution [0.1 M HEPES and 1.1 N sodium citrate (pH

7.5)] in a sitting drop tray with 500 μL of the reservoir solution. Crystals were observed after being incubated for 3 days at 12 $^{\circ}\text{C}$ and harvested after growing for 4 weeks. Sodium citrate itself is a cryoprotectant, and hence, there was no need for any additional cryoprotectant.³² Diffraction data were acquired on frozen crystals (100 K) using a Rigaku FR-E generator with a Cu rotating anode and a Saturn 944 CCD detector. Although we could readily form crystals in the presence of ADP with dGMP or AZTMP, these crystals diffracted poorly and were not pursued further.

Structure Determination, Model Building, and Refinement. The CCP4 software package³³ was used to perform the different steps involved in arriving at the final structure. Indexing and integration of the reflections were performed using iMosflm 7.2.0.³⁴ Scaling and truncation of the data were performed using Aimless.³⁵ The sequence of CaTMPK is 52% identical to that of the thymidylate kinase from *S. cerevisiae*, which has several known structures deposited in the PDB. CHAINSAW³⁶ was used to generate an initial search model based on the sequence alignment with *S. cerevisiae* TMPK complexed with the bisubstrate inhibitor Ap_3T (PDB entry 3TMK³⁷). This model was used as a search model to perform molecular replacement using Phaser.³⁸ The top rotation function score was 27.84 ($Z = 6.46$), and the top translation function score was 132.32 ($Z = 11.04$). The R values after 20 cycles of refinement of the initial molecular replacement solution with REFMAC5³⁹ were 0.199 and 0.263 for R_{factor} and R_{free} , respectively. Model building was performed using Coot,⁴⁰ and structures were refined using REFMAC5³⁹ after each manual adjustment of the model. At the end of model building, the model was analyzed by PDB-REDO⁴¹ for suggestions about the modification of rotamers, Asn/Gln flips, and removal of water molecules. One rotamer change was justified by the density; eight Asn/Gln residues were flipped, and one water molecule was removed. The final model has an R_{factor} of 0.168 and an R_{free} of 0.223. The statistics of the data and final model are given in Table S1.

Activity Assay Using Proton NMR. One-dimensional proton (^1H) NMR was used to monitor the activity of CaTMPK. The assay depends on the change in the chemical shift of the H6 proton (TMP and AZTMP) or the H8 proton (dGMP) of the nucleobases upon the addition of the second phosphate group. The assay reaction included 1 mM ATP as the phosphate donor, phosphate acceptor, TMP (1 mM), or AZTMP (1 mM), or dGMP (5 mM), 10 mM MgCl_2 , 1 mM potassium acetate, and 10% D_2O . A ^1H spectrum of the reaction mix was acquired before addition of CaTMPK to the reaction mix. A series of NMR spectra were acquired every 3.3 min for up to 164 min. The area of the proton line corresponding to the monophosphate forms of the acceptor molecule was plotted against time to calculate the initial rates of catalysis for each of the three substrates, assuming an exponential fit. The catalytic rate constant, k_{CAT} , was obtained by dividing the rate by the enzyme concentration. Reactions with TMP as the phosphate acceptor were performed with 0.01 μM enzyme. The lower activity toward AZTMP and dGMP required the use of a higher enzyme concentration for these substrates, 0.1 μM for AZTMP and 10 μM for dGMP, to allow the production of significant amounts of product during the assay.

Activity Assay Using Coupled Reactions. The NADH coupled enzyme activity assay³¹ was used to measure the activity of CaTMPK with the different phosphate acceptors

(TMP, AZTMP, and dGMP). The reaction mixture consisted of 50 mM Tris-HCl (pH 7.4), 50 mM KCl, 10 mM MgCl_2 , 0.5 mM phosphoenolpyruvate, 0.15 mM NADH, 5 units/mL pyruvate kinase, and 5 units/mL lactate dehydrogenase. The reaction was initiated by adding the enzyme, and the reaction rate was measured by monitoring the decrease in the NADH concentration at 340 nm. The K_{M} values for TMP, AZTMP, and dGMP were obtained by varying the concentration of these substrates using 1 mM ATP. This concentration of ATP is commonly used when characterizing the activity of TMPKs toward different substrates (see refs 22 and 42). The K_{M} for ATP was obtained under saturating TMP conditions (200 μM $\approx 33K_{\text{M}}$). The K_{M} values for different substrates were obtained by direct fitting to the Michaelis–Menten velocity equation: $v = [\text{E}_{\text{TOT}}]k_{\text{CAT}}[\text{S}]/(K_{\text{M}}^{\text{APP}} + [\text{S}])$. The k_{CAT} values reported here have not been corrected for effects of nonsaturating levels of ATP; these k_{CAT} values should be increased by $1 + K_{\text{M}}^{\text{ATP}}/[\text{ATP}]$, or in this case by a factor of 1.26, to give the equivalent k_{CAT} at a saturating level of ATP.

Binding of dGMP to CaTMPK As Determined by NMR Chemical Shift Perturbation. Perdeuterated, ILV-methyl-labeled samples of CaTMPK were prepared by growth in D_2O minimal medium⁴³ with ketovalerate and ketobutyrate methyl ^1H - and ^{13}C -labeled precursors (Cambridge Isotopes), essentially as described by Goto and Kay⁴⁴ with modifications described in ref 45. ^1H – ^{13}C HMQC spectra were acquired at 600 MHz (^1H) on a 200 μM sample of CaTMPK, in the presence of 1 mM ADP and 10 mM Mg^{2+} and increasing concentrations of dGMP from 0 to 4 mM. The chemical shift changes in the methyl resonances that were induced by dGMP were fit to the standard single-site binding equation: $Y = [\text{dGMP}]/(K_{\text{D}} + [\text{dGMP}])$.

Modeling the Binding of AZTMP and dGMP in the Active Site. The model for AZTMP bound at the CaTMPK active site in the presence of ADP was generated by replacing the TMP with AZTMP in the crystal structure. The coordinates of dGMP bound to the monomer were modeled on the basis of the dGMP coordinates in the *P. falciparum* TMPK–dGMP complex²² (PDB entry 2WWG). The *C. albicans* dimer containing dGMP was generated using crystallographic symmetry and energy-minimized using NAMD.⁴⁶ Briefly, the psf file was generated using the top_all27 topology file, and the parameters were obtained from the par_all27 file. The molecule was solvated and charge-neutralized using VMD and subjected to 1000 minimization steps. A similar process was used to model dGMP bound to the human enzyme, beginning with the structure of the TMP–ADP complex (PDB entry 1E2D²).

RESULTS AND DISCUSSION

Substrate Specificity of CaTMPK. The activity of CaTMPK toward TMP, AZTMP, and dGMP was measured using a traditional coupled assay and the new NMR-based assay described here. The NMR assay was used to initially test the ability of CaTMPK to catalyze the addition of a second phosphate group to TMP, AZTMP, and dGMP. The results show that the enzyme can use all three monophosphates as substrates (see Figure 4). To obtain accurate values for k_{CAT} from the NMR-based assay, it was necessary to add sufficient enzyme to sustain a rate of reaction similar to that shown in Figure 4 for TMP. Consequently, an approximately 10-fold higher enzyme concentration was used for data acquired with AZTMP, and a 1000-fold higher value was used when dGMP was the substrate. The maximum reaction rates that were

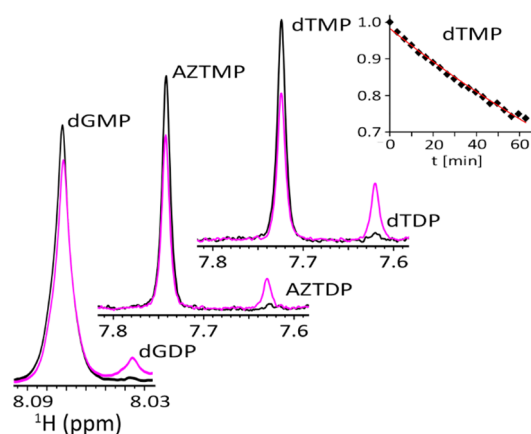


Figure 4. Activity of CaTMPK determined by ^1H NMR spectroscopy. The indicated substrate, dGMP at 5 mM, AZTMP at 1 mM, or TMP at 1 mM, was mixed with ATP (1 mM), Mg^{2+} (10 mM), and CaTMPK, and proton NMR spectra were recorded every 3.3 min. The spectra show the resonance from H8 on dGMP or H6 on AZTMP or TMP. These protons show a change in chemical shift upon the addition of a phosphate. The black trace corresponds to $t = 3.3$ and the cyan trace to the data point at $t = 164$ min (dGMP) or $t = 33$ min (AZTMP and TMP). The inset shows a plot of the normalized substrate intensity vs time for TMP (\blacklozenge) with the best fit to an exponential function [$I(t) = e^{-kt}$] shown as the red line.

obtained with the NMR-based assay were significantly higher for TMP and AZTMP than for the coupled assay (see Table 1), while the rates were essentially the same for both assays when dGMP was the phosphate acceptor. This suggests that TMP and AZTMP may slightly interfere with the enzymes that couple ADP production to NADH reduction. Although the NMR-based assay was used here to measure k_{CAT} for different substrates, it could be adapted to library screening in which a mixture of 20–50 compounds are screened in a single sample. Resonance lines from the compounds that overlap with the TMP H6 resonance can be easily removed by difference spectroscopy.

Although the NMR-based assay provides a convenient method for obtaining k_{CAT} , it is not ideal for K_{M} determinations because of the necessity to acquire velocity data with different substrate concentrations. Consequently, the K_{M} values were obtained with the coupled assay (see Table 1). The K_{M} for ATP, in the presence of a saturating level of (200 μM) TMP, was $260 \pm 20 \mu\text{M}$, as determined from the coupled assay. This is similar to the values for TMPK from *S. cerevisiae*, which was found to be 190 μM with TMP as the substrate and 300 μM with AZTMP as the substrate,¹⁰ but higher than the reported

value for vaccinia TMPK of 130 μM ,⁴² or human TMPK, which range from 5 to 69 μM , depending on the substrate.⁴⁷ The K_{M} values for TMP, AZTMP, and dGMP for CaTMPK are listed in Table 1, along with kinetic data from other eukaryotic and viral thymidylate kinases.

CaTMPK is very effective at using TMP as a substrate, showing a k_{CAT} that is surpassed only by the enzyme from *S. cerevisiae* and a small K_{M} , similar to that found for the human enzyme. Although the CaTMPK enzyme is 3-fold less effective toward AZTMP than the enzyme from *P. falciparum* (0.5 s^{-1} vs 1.8 s^{-1}), CaTMPK is 30-fold more effective at phosphorylating AZTMP than the human enzyme, showing an only 20-fold decrease in rate with respect to TMP, in contrast to the 70-fold difference associated with the human enzyme.¹¹

CaTMPK shows demonstrable activity toward dGMP, based on both the direct NMR assay and the coupled assay. The K_{M} for dGMP was considerably higher than the values found for PfTMPK. Consequently, we independently verified the high K_{M} for dGMP by measuring binding to the ADP– Mg^{2+} complex using NMR chemical shift perturbations and obtained a value of 2.7 mM for K_{D} under these conditions (see Figure S1). The low activity of the CaTMPK toward dGMP is in contrast with that of the enzyme from *P. falciparum* that can utilize dGMP almost as effectively as TMP. Consequently, it is unlikely that CaTMPK plays a significant role in converting dGMP to dGDP *in vivo*.

Structure of CaTMPK. The structure of CaTMPK in complex with ADP and TMP was determined by molecular replacement to a resolution of 2.45 Å. The data and refinement statistics are listed in Table S1. The quality of the data and final phases was sufficiently high to identify the location of the single cysteine based on anomalous scattering from the sulfur (see Figure S2). There is one residue (Tyr93) in the unfavorable region of the Ramachandran plot and one residue, Arg92, in an allowed region that does not contain a favored region (see Figure S3). The electron density covering these two residues clearly shows the orientation of the C=O groups on both residues, suggesting that the unfavorable ϕ and ψ values have been modeled correctly. The distortion of the backbone conformation for these two residues appears to be due to hydrogen bonds between Arg92 and Gly97 and between Tyr93 and Ile9 (see Figure S3).

The overall structure of the *C. albicans* enzyme contains a five-stranded β -sheet at the core surrounded by α -helices. The dimer interface mainly consists of a part of helix $\alpha 3$ (DQAAHLLFSANRW) with the hydrophobic side chains of W, L, and A oriented toward the interface. The enzyme is structurally homologous to TMPKs from other organisms, with

Table 1. Summary of Enzyme Kinetic Parameters for Thymidylate Kinases^a

enzyme	TMP		AZTMP		$k_{\text{CAT}}^{\text{TMP}}/k_{\text{CAT}}^{\text{AZTMP}}$	dGMP	
	k_{CAT} (s^{-1})	K_{M} (μM)	k_{CAT} (s^{-1})	K_{M} (μM)		k_{CAT} (s^{-1})	K_{M}
hTMPK	0.7	5	0.01	12	70	NR ^b	NR ^b
yTMPK	35	9	0.175	6	200	NR ^b	NR ^b
PfTMPK	4.9	10.7	1.80	9.1	2.7	4.7	12.6 μM
VaccTMPK	2.2	20	0.11	85	20	0.58	240 μM
CaTMPK (NADH coupled assay)	6.9 ± 0.1	6.2 ± 1.4	0.3 ± 0.03	4.5 ± 1.6	22	0.008 ± 0.0005	$1.07 \pm 0.1 \text{ mM}$
CaTMPK (NMR assay)	8.7 ± 0.3	ND ^c	0.5 ± 0.03	ND ^c	17.4	0.006 ± 0.0008	ND ^c

^aValues for TMPK from human (hTMPK) are from ref 47, *S. cerevisiae* (yTMPK) from ref 10, *P. falciparum* (PfTMPK) from ref 22, and vaccinia virus (VaccTMPK) from ref 42. The standard errors for the values reported for CaTMPK were based on triplicate measurements. ^bNot reported. ^cNot determined.

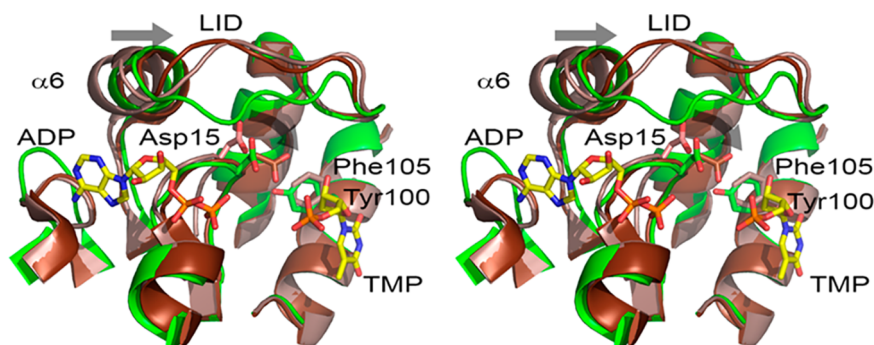


Figure 5. Comparison of the active site region in CaTMPK and hTMPK. This crossed-stereo diagram shows the active site of CaTMPK (ADP/TMP, green) and hTMPK with either ADP/TMP (PDB entry 1E2D,² dark salmon) or Ap₅T (PDB entry 1E2Q,² brown). In the human enzyme, the active site in the ADP/TMP complex is partially closed. Complete closure is seen when Ap₅T is bound, as indicated by a shift of helix $\alpha 6$ above ADP and the movement of Asp15 to become adjacent to the 3'-OH of TMP (gray arrows). The *C. albicans* ADP/TMP complex is more similar to the human Ap₅T structure, in the position of both the helix and the Asp15 residue, indicating almost complete closure in the presence of ADP and TMP. A difference between the human and *C. albicans* TMPK is the replacement of Phe105 on the human enzyme with Tyr100 in the *C. albicans* enzyme. The Tyr100 side chain occupies the same position as Phe105 and is in the same position as the Phe105Tyr substitution in the human enzyme that confers enhanced reactivity to AZTMP.

RMSD values that vary from 0.6 Å for *S. cerevisiae* to 3.88 Å for TMPK from *Brukholderia thailandensis* (Table S2), mirroring the level of sequence similarity (see Figures S6 and S7).

The P-loop of the *C. albicans* enzyme, like the human, yeast, and *Plasmodium* TMPKs, possesses the catalytically crucial Arg and Asp residues. Figure 5 compares the active site of the CaTMPK (ADP and TMP complex) with the hTMPK bound to either ADP/TMP or the bisubstrate analogue Ap₅T. In the human enzyme, the active site of the TMP/ADP-bound complex is only partially closed and achieves a closed and fully active configuration only upon binding of Ap₅T. The positioning of the P-loop and the orientation of the catalytically important Asp15 residue in the P-loop, as well as the helix adjacent to the LID region ($\alpha 6$), are different between the two complexes of hTMPK. Both the P-loop and helix $\alpha 6$ of the CaTMPK ADP/TMP complex are shifted with respect to the hTMPK–ADP/TMP structure and more closely resemble the closed active site configuration of the hTMPK–Ap₅T complex.

In contrast to the P-loop and LID region, most of the other secondary structural elements in human TMPK are not significantly altered by the presence of different ligands in the active site. These elements include helices $\alpha 5$ and $\alpha 8$ and strand $\beta 5$ just before helix $\alpha 8$ (Figure 6). These secondary structures are shifted in the CaTMPK structure relative to that of hTMPK; the largest differences in C_{α} positions are 2.08 Å ($\alpha 5$), 3.02 Å ($\beta 5$), and 4.64 Å ($\alpha 8$). The difference in the position of helix $\alpha 5$ in CaTMPK is likely due to the increased length of the segment leading to $\alpha 5$; this segment contains the additional 15 residues not found in the human enzyme. Strand $\beta 5$ and helix $\alpha 8$ are below the ATP binding site, and their shift is due to numerous sequence differences in this region of the protein.

Sequence alignment of the CaTMPK against the human enzyme shows the presence of 15 extra residues in the loop between helices $\alpha 4$ and $\alpha 5$ (Ca-loop). In the CaTMPK enzyme, this loop is above the active site and contacts the LID region, while in the human enzyme, it is too distant from the LID region to form any contacts (see Figure 1). Although the tip of this loop has relatively high *B* factors [~ 70 Å² (Figure S4)], it is well-structured. The structuring of the Ca-loop appears to be due to a network of inter- and intrasubunit hydrogen bonding interactions (Figure 7) and not lattice

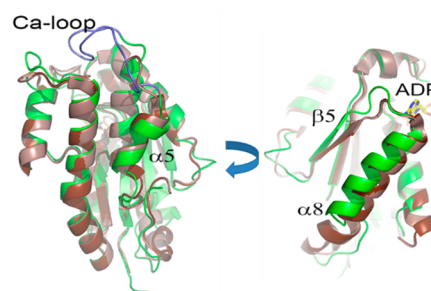


Figure 6. Differences between conserved structural elements in CaTMPK and hTMPK. The location of helix $\alpha 5$ (left) and strand $\beta 5$ and helix $\alpha 8$ (right) are unaffected by changes in the bound ligand in hTMPK structures; the structures of these elements in TMP/ADP (PDB entry 1E2D, dark salmon) or Ap₅T (PDB entry 1E2Q, brown) are superimposable. These structural elements in CaTMPK (green) are displaced from their positions found in hTMPK. The bound ADP is rendered as sticks and colored CPK with the carbon atoms colored yellow. The Ca-loop indicates the 15 additional residues not found in the human TMPK sequence and is colored slate blue.

packing effects (see Figure S5). The *N* ϵ atom on the side chain of Lys118 forms hydrogen bonds with the side chain of Ser113 (2.82 Å, N–O) and the carbonyl oxygen of Phe107 (2.84 Å, N–O) and weaker interactions with the main-chain C=O groups from Lys104 (3.5 Å) and Gly115 (3.8 Å) (not shown in Figure 7). In addition to the partial negative charges that are contributed by residues 104, 107, 113, and 115, there is also a formal negative charge from Asp60; its O $\delta 2$ atom is 4.88 Å from the *N* ϵ atom of Lys118. The negative electrostatic potential at the position of the *N* ϵ atom of Lys118 stabilizes the insertion of the lysine side chain into this pocket and provides stability for the entire Ca-loop. The interaction with Lys118 appears to be completely conserved in TMPK from *C. albicans*, *C. dubliniensis*, and *C. orthopsilosis*.

There are three residues in the Ca-loop that are conserved among all *Candida* species that contain the same loop size (see Figure 3B), Ile112, Ser113, and Leu121. Ile112 and Leu121 stabilize the Ca-loop by forming a small hydrophobic core. As described above, Ser113 forms hydrogen bonding interactions with Lys118 in the *C. albicans* enzyme and likely does the same in the enzymes from *C. dubliniensis* and *C. orthopsilosis*. In *C.*

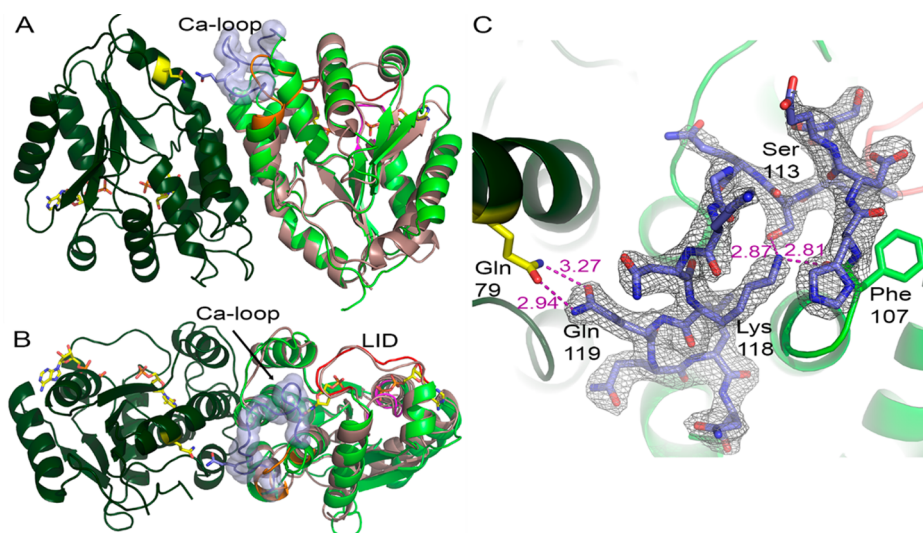


Figure 7. Overlay of CaTMPK with hTMPK and electron density of the Ca-loop. Panels A (side view) and B (top view) show the CaTMPK dimer with the Ca-loop colored slate blue and highlighted in blue, the LID colored red, and the P-loop colored cyan for the right monomer. The left monomer is colored dark green, except for the Gln residue (position 79) that is responsible for stabilizing the Ca-loop by intersubunit interactions, which is colored yellow. Bound nucleotides (ADP and TMP) are shown with their carbons colored yellow. One monomer of the human enzyme is shown aligned with the right monomer of CaTMPK, colored dark salmon. The region of the human enzyme that corresponds to the Ca-loop is colored orange. Panel C shows the electron density from the $2F_o - F_c$ map for the Ca-loop after final refinement. The hydrogen bonding interactions that stabilize the structure of the Ca-loop are illustrated with magenta dotted lines. Residues 108–122 (colored slate blue) from one subunit are ordered with clearly interpretable electron density for the main chain and most of the side-chain atoms (contoured at 1.2σ). Stabilization occurs due to hydrogen bonding between Gln119 on one subunit and Gln79 on the other subunit, with distances of 2.94 and 3.27 Å. Hydrogen bonding within the Ca-loop and between the side chain of Lys118 and the side chain of Ser113 (2.87 Å) and the main chain of Phe107 (2.81 Å) also stabilize the Ca-loop.

tropicalis, a lysine at the next position of the chain may form the same interactions. In addition to these intrasubunit hydrogen bonding and electrostatic interactions, Gln119 on the Ca-loop also participates in hydrogen bonding interactions with Gln79 of the other subunit. This interaction appears to be conserved in *C. dubliniensis* and could also occur in *C. tropicalis* with a displacement of Gln120 to the position occupied by Gln119 in the other enzymes. In conclusion, the Ca-loop appears to be stabilized by a combination of hydrophobic, hydrogen bonding, and electrostatic interactions that are conserved in a number of *Candida* species.

Although the Ca-loop is not directly involved in binding of substrates, it interacts with the LID region of the enzyme (see Figure 8). Ile112 has close contacts with Arg160, Leu163, and Phe166. In addition, Thr111 in the Ca-loop hydrogen bonds with Arg160, which is conserved in TMPKs (see Figure 2). This suggests that the structure of the Ca-loop is positioned such that it could affect the mechanism of the enzyme because of the presumptive movement of the LID during the catalytic cycle.

Catalytic Activity toward AZTMP and dGMP. CaTMPK is highly active against AZTMP and also shows activity toward dGMP (see Table 1 and Figure 4). Consequently, both of these substrates must be able to bind in the active site. The crystal structure of the TMP bound to CaTMPK shows a water molecule (Figure 9A) that participates in a hydrogen bonding interaction with the 3'-OH of the TMP. The bulky azido group on AZTMP can easily be accommodated in place of TMP by the displacement of the water by the 3'-azido group (Figure 9B), allowing AZTMP to bind with an affinity similar to that of TMP. The high catalytic activity toward AZTMP by CaTMPK and PftMPK, relative to hTMPK, may be due to the substitution of Phe108 in the human enzyme with Tyr100 in

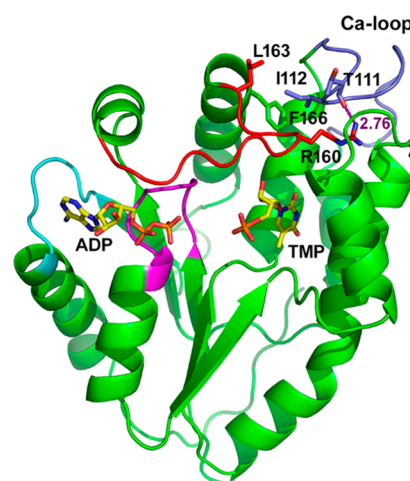


Figure 8. Interactions of the Ca-loop with the LID region. Thr111 and Ile112 in the Ca-loop (slate blue) interact with the LID region (red). The C=O group of Thr111 forms a hydrogen bond with Arg160 (2.76 Å), and Ile112 forms hydrophobic and/or van der Waals interactions with Arg160, Leu163, and Phe166.

CaTMPK or Tyr107 in PftMPK. This Tyr residue can form two main-chain hydrogen bonds with the P-loop that contains a critical Asp residue, enhancing the stability of the closed form of the enzyme (see Figure 5). This hypothesis is supported by the fact that changing the equivalent Phe to Tyr in the human enzyme greatly enhances the catalytic efficiency toward AZTMP, presumably facilitating the closure of the P-loop when AZTMP is the substrate.^{11,48}

Although dGMP is substantially larger than TMP, it is possible to accommodate the bulkier purine ring in the TMP

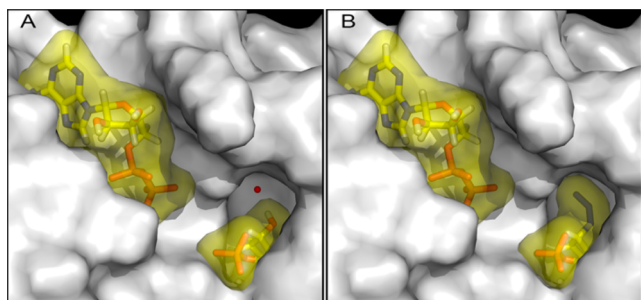


Figure 9. Binding of TMP and AZTMP to CaTMPK. Panel A shows ADP (top left) and TMP (bottom right) bound on the surface of the enzyme. A water molecule (red sphere) forms a hydrogen bond to the 3'-OH of TMP. Panel B shows AZTMP replacing TMP. The 3'-azido group in the AZTMP complex displaces the water molecule.

site by rotation around the N-glycosidic linkage. The NAMD-generated models of dGMP bound at the active site of hTMPK and CaTMPK are shown in panels A and B of Figure 10, respectively. The structure of the dGMP–PfTMPK complex, as determined by X-ray diffraction (PDB entry 2WWG), is shown in Figure 10C.²² Four residues in the active site of PfTMPK, His71, Arg78, Ser108, and Tyr 153, form H-bond interactions with the bound dGMP. These interactions are strikingly similar in both hTMPK and the CaTMPK enzymes, where a His residue (position 69 or 64), an Arg residue (position 76 or 71), a Thr residue (position 106 or 101), and a Tyr residue (position 151 or 161) appear to be able to form a similar network of hydrogen bonds with the bound dGMP substrate. Although the interactions of the bound dGMP appear to be similar in each of these TMPKs, their ability to phosphorylate dGMP is quite different. The human TMPK is reported not to bind dGMP;^{23,24} CaTMPK shows a very slow rate of dGMP phosphorylation, while PfTMPK can readily phosphorylate dGMP (see Table 1). Replacing the Ser residue at position 108 in PfTMPK with a bulkier Thr residue in the human and *C. albicans* enzymes may impede subtle rearrangements in the active site that are required for high-affinity binding of dGMP and its subsequent catalysis. However, altering Ser108 to Thr in PfTMPK has a negligible effect on k_{CAT} toward dGMP and increases the K_{M} for dGMP from $30 \pm 7.2 \mu\text{M}$ to only $38 \pm 7.8 \mu\text{M}$,⁴⁹ suggesting that local conformational restrictions due to a Thr residue at this position (position 106 in hTMPK and position 101 in CaTMPK) may not be the major determinant of poor activity toward dGMP. Thermodynamic measure-

ments⁴⁹ for the binding of TMP and dGMP to PfTMPK suggest that the *P. falciparum* enzyme can utilize dGMP as a substrate because of enhanced flexibility during the catalytic cycle. Although both TMP and dGMP bind with near equal affinity to PfTMPK ($\Delta G^\circ = -6.4 \text{ kcal/mol}$), the binding of TMP involves a change in enthalpy (-42.0 kcal/mol) much larger than that of dGMP (-14.1 kcal/mol). Consequently, dGMP binding leads to a smaller decrease in entropy ($T\Delta S^\circ$ values of -7.6 and -35 kcal/mol for TMP), suggesting that the dGMP–enzyme complex has retained additional conformational flexibility after dGMP has bound and this flexibility is required for high activity.

The TMPK from vaccinia virus can also readily phosphorylate dGMP; its k_{CAT} toward dGMP is only 4-fold lower than the k_{CAT} for TMP. The structure of PfTMPK is sufficiently similar to that of VaccTMPK (RMSD for alignment of 0.56 Å) that it is possible to directly compare their active site regions to develop an understanding of why VaccTMPK is also active against dGMP. Figure 11 shows a superposition of the dGMP–

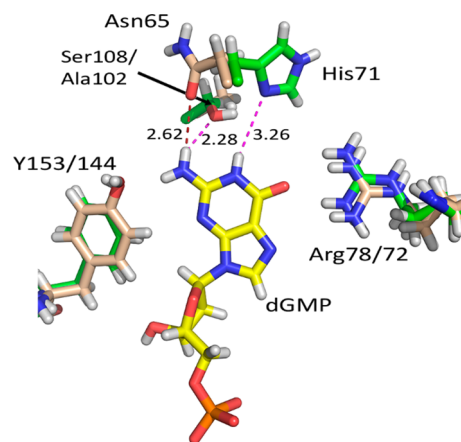


Figure 11. dGMP binding in PfTMPK and VaccTMPK. PfTMPK is colored green (C), blue (N), and red (O) with the bound dGMP colored yellow (C), blue (N), and red (O) (image generated from PDB entry 2WWG).²² The structure of VaccTMPK complexed with TMP (PDB entry 2V54⁵⁰) was aligned with 2WWG using Pymol and is colored salmon (C), blue (N), and red (O). If the residues are equivalent, the first number refers to the location in PfTMPK and the second to that in VaccTMPK; e.g., the Tyr residue is at position 153 in PfTMPK and position 144 in VaccTMPK.

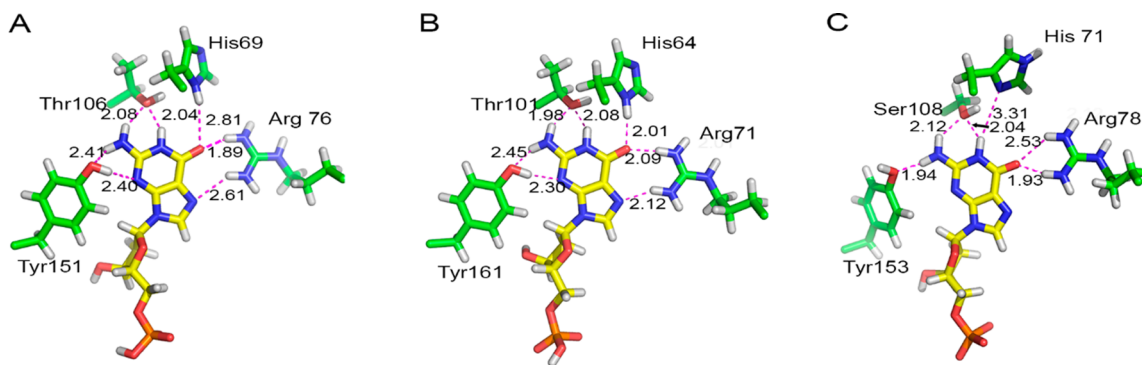


Figure 10. dGMP in the TMP binding site. dGMP bound in the TMP binding site of (A) the human enzyme, (B) the *C. albicans* enzyme, and (C) the enzyme from *P. falciparum*. The structure of the human and *C. albicans* enzyme was generated by modeling, and the structure of the *P. falciparum* enzyme was obtained from PDB entry 2WWG.²²

interacting residues in PfTMPK with spatially equivalent residues found in VaccTMPK. The interactions between dGMP and a Tyr and Arg residue in the dGMP binding site appear to be identical in both enzymes. In contrast, His71 and Ser108 in PfTMPK are replaced with Asn65 and Ala102 in VaccTMPK. These substitutions cause the loss of two hydrogen bonds to dGMP in VaccTMPK, one to the His and one to the Ser. However, the replacement of Ser108 with Ala appears to allow the side chain of Asn65 to swing closer to the bound dGMP, such that the two missing hydrogen bonds in PfTMPK are replaced by a single hydrogen bond to Asn65 in VaccTMPK. The change in the number of hydrogen bonds is consistent with the change in K_M , where PfTMPK shows a K_M that is lower than that of VaccTMPK. Unfortunately, there are no thermodynamic data on the binding of TMP and dGMP to VaccTMPK to determine whether entropy is also contributing to its high activity toward dGMP.

In summary, the results presented here show that the TMPK from *C. albicans* possesses a number of unique structural and functional features that distinguish it from its human counterpart. In terms of substrate specificity, the TMPK from *C. albicans* is more proficient at phosphorylating AZTMP than the human enzyme is. The enhanced activity toward AZTMP may be due to the presence of Tyr100 in CaTMPK instead of the Phe residue in the human enzyme. Although CaTMPK is active toward dGMP, while the human enzyme is not, the activity of CaTMPK is much lower than those of PfTMPK and VaccTMPK enzymes. The low activity of CaTMPK and the lack of activity in the human enzyme may be due to the presence of a bulkier Thr residue in these kinases, which is replaced by a smaller Ser residue in the enzyme from *P. falciparum*. Differences in the intrinsic dynamics of these enzymes may also affect their ability to utilize dGMP as a substrate.

A significant structural difference between the CaTMPK and thymidylate kinases from unrelated species is the length of the loop connecting helices $\alpha 5$ and $\alpha 6$. This 15-residue "Ca-loop" is highly structured because of several conserved inter- and intrasubunit interactions, and a number of these interactions appear to be conserved among different *Candida* species. Although the Ca-loop is not directly involved in the binding of substrates, it interacts with the LID region through a conserved Ile residue (I112), as well as main-chain hydrogen bonds, indicating that the structure of the Ca-loop is positioned such that it could affect the catalytic mechanism of the enzyme.

CaTMPK is a potential drug target for antifungal drug discovery for a number of reasons. First, it shows several structural differences compared to its human counterpart. These include the Ca-loop, as well as significant shifts in the location of helices and strands. These structural differences could form potential binding sites for allosteric inhibitors. Second, the fact the CaTMPK can utilize dGMP as a substrate suggests that competitive inhibitors that resemble purine nucleosides may preferentially bind to CaTMPK versus the human enzyme.

■ ASSOCIATED CONTENT

● Supporting Information

The Supporting Information is available free of charge on the ACS Publications website at DOI: [10.1021/acs.biochem.7b00498](https://doi.org/10.1021/acs.biochem.7b00498).

Table listing statistics for diffraction data and the final model; table of RMSDs between *C. albicans* TMPK and TMPKs from other species; binding affinity of dGMP, measured using chemical shift perturbation; anomalous electron density map, Ramachandran plot, and electron density map associated with Ramachandran outliers; graphical representation of main-chain temperature factors; crystal contacts that influence the structure of the Ca-loop; and a phylogenetic tree and sequence alignments for TMPKs with known structures (PDF)

■ Accession Codes

Atomic coordinates and crystallographic structure factors for the *C. albicans* TMPK-ADP-TMP-Mg²⁺ complex have been deposited as Protein Data Bank entry SUIV.

■ AUTHOR INFORMATION

Corresponding Author

*E-mail: rule@andrew.cmu.edu. Phone: 412-268-1839.

ORCID

Gordon S. Rule: [0000-0002-4396-3363](https://orcid.org/0000-0002-4396-3363)

Funding

This work was supported by a Mellon College of Science (Carnegie Mellon University) award to G.S.R.

Notes

The authors declare no competing financial interest.

■ ACKNOWLEDGMENTS

We thank Mr. Doowon Lee for assistance in collecting diffraction data and Mr. Virgil Simplaceanu for assistance with NMR.

■ ABBREVIATIONS

HEPES, 4-(2-hydroxyethyl)-1-piperazineethanesulfonic acid; LB, Luria-Bertani; IPTG, isopropyl β -D-thiogalactoside; TEV, tobacco etch virus; DTT, 1,4-dithiothreitol; EDTA, ethylenediaminetetraacetic acid; Tris, tris(hydroxymethyl)aminomethane; PDB, Protein Data Bank.

■ REFERENCES

- (1) Reichard, P. (1988) Interactions between deoxyribonucleotide and DNA synthesis. *Annu. Rev. Biochem.* 57, 349–374.
- (2) Ostermann, N., Schlichting, I., Brundiers, R., Konrad, M., Reinstein, J., Veit, T., Goody, R. S., and Lavie, A. (2000) Insights into the phosphoryltransfer mechanism of human thymidylate kinase gained from crystal structures of enzyme complexes along the reaction coordinate. *Structure* 8, 629–642.
- (3) *The PyMOL Molecular Graphics System*, version 1.8 (2015) Schrodinger, LLC, Portland, OR.
- (4) Edgar, R. C. (2004) MUSCLE: multiple sequence alignment with high accuracy and high throughput. *Nucleic acids research* 32, 1792–1797.
- (5) Robert, X., and Gouet, P. (2014) Deciphering key features in protein structures with the new ENDscript server. *Nucleic Acids Res.* 42, W320–W324.
- (6) Huang, S.-H., Tang, A., Drisco, B., Zhang, S.-Q., Seeger, R., Li, C., and Jong, A. (1994) Human dTMP Kinase: Gene Expression and Enzymatic Activity Coinciding with Cell Cycle Progression and Cell Growth. *DNA Cell Biol.* 13, 461–471.
- (7) Ke, P.-Y., Kuo, Y.-Y., Hu, C.-M., and Chang, Z.-F. (2005) Control of dTTP pool size by anaphase promoting complex/cyclosome is essential for the maintenance of genetic stability. *Genes Dev.* 19, 1920–1933.

- (8) Hu, C. M., Yeh, M. T., Tsao, N., Chen, C. W., Gao, Q. Z., Chang, C. Y., Lee, M. H., Fang, J. M., Sheu, S. Y., Lin, C. J., Tseng, M. C., Chen, Y. J., and Chang, Z. F. (2012) Tumor cells require thymidylate kinase to prevent dUTP incorporation during DNA repair. *Cancer Cell* 22, 36–50.
- (9) Liu, Y., Marks, K., Cowley, G. S., Carretero, J., Liu, Q., Nieland, T. J., Xu, C., Cohoon, T. J., Gao, P., Zhang, Y., Chen, Z., Altabef, A. B., Tchaicha, J. H., Wang, X., Choe, S., Driggers, E. M., Zhang, J., Bailey, S. T., Sharpless, N. E., Hayes, D. N., Patel, N. M., Janne, P. A., Bardeesy, N., Engelman, J. A., Manning, B. D., Shaw, R. J., Asara, J. M., Scully, R., Kimmelman, A., Byers, L. A., Gibbons, D. L., Wistuba, II, Heymach, J. V., Kwiatkowski, D. J., Kim, W. Y., Kung, A. L., Gray, N. S., Root, D. E., Cantley, L. C., and Wong, K. K. (2013) Metabolic and functional genomic studies identify deoxythymidylate kinase as a target in LKB1-mutant lung cancer. *Cancer Discovery* 3, 870–879.
- (10) Lavie, A., Schlichting, I., Vetter, I. R., Konrads, M., Reinstein, J., and Goody, R. S. (1997) The bottleneck in AZT activation. *Nat. Med.* 3, 922–924.
- (11) Brundiers, R., Lavie, A., Veit, T., Reinstein, J., Schlichting, I., Ostermann, N., Goody, R. S., and Konrad, M. (1999) Modifying human thymidylate kinase to potentiate azidothymidine activation. *J. Biol. Chem.* 274, 35289–35292.
- (12) Johnson, A. A., Ray, A. S., Hanes, J., Suo, Z., Colacino, J. M., Anderson, K. S., and Johnson, K. A. (2001) Toxicity of Antiviral Nucleoside Analogs and the Human Mitochondrial DNA Polymerase. *J. Biol. Chem.* 276, 40847–40857.
- (13) Sato, T., Neschadim, A., Lavie, A., Yanagisawa, T., and Medin, J. A. (2013) The engineered thymidylate kinase (TMPK)/AZT enzyme-prodrug axis offers efficient bystander cell killing for suicide gene therapy of cancer. *PLoS One* 8, e87811.
- (14) Deville-Bonne, D., El Amri, C., Meyer, P., Chen, Y., Agrofoglio, L. A., and Janin, J. (2010) Human and viral nucleoside/nucleotide kinases involved in antiviral drug activation: structural and catalytic properties. *Antiviral Res.* 86, 101–120.
- (15) Martinez-Botella, G., Breen, J. N., Duffy, J. E., Dumas, J., Geng, B., Gowers, I. K., Green, O. M., Guler, S., Hentemann, M. F., Hernandez-Juan, F. A., Joseph-McCarthy, D., Kawatkar, S., Larsen, N. A., Lazari, O., Loch, J. T., Macritchie, J. A., McKenzie, A. R., Newman, J. V., Olivier, N. B., Otterson, L. G., Owens, A. P., Read, J., Sheppard, D. W., and Keating, T. A. (2012) Discovery of selective and potent inhibitors of gram-positive bacterial thymidylate kinase (TMK). *J. Med. Chem.* 55, 10010–10021.
- (16) Martinez-Botella, G., Loch, J. T., Green, O. M., Kawatkar, S. P., Olivier, N. B., Boriack-Sjodin, P. A., and Keating, T. A. (2013) Sulfonypiperidines as novel, antibacterial inhibitors of Gram-positive thymidylate kinase (TMK). *Bioorg. Med. Chem. Lett.* 23, 169–173.
- (17) Cui, H., Carrero-Lerida, J., Silva, A. P., Whittingham, J. L., Brannigan, J. A., Ruiz-Perez, L. M., Read, K. D., Wilson, K. S., Gonzalez-Pacanowska, D., and Gilbert, I. H. (2012) Synthesis and evaluation of alpha-thymidine analogues as novel antimalarials. *J. Med. Chem.* 55, 10948–10957.
- (18) Van Poecke, S., Munier-Lehmann, H., Helynck, O., Froeyen, M., and Van Calenbergh, S. (2011) Synthesis and inhibitory activity of thymidine analogues targeting Mycobacterium tuberculosis thymidine monophosphate kinase. *Bioorg. Med. Chem.* 19, 7603–7611.
- (19) Familiar, O., Munier-Lehmann, H., Ainsa, J. A., Camarasa, M. J., and Perez-Perez, M. J. (2010) Design, synthesis and inhibitory activity against Mycobacterium tuberculosis thymidine monophosphate kinase of acyclic nucleoside analogues with a distal imidazoquinolinone. *Eur. J. Med. Chem.* 45, 5910–5918.
- (20) Kandeel, M., and Kitade, Y. (2011) The substrate binding preferences of Plasmodium thymidylate kinase. *Biol. Pharm. Bull.* 34, 173–176.
- (21) Lavie, A., Ostermann, N., Brundiers, R., Goody, R. S., Reinstein, J., Konrad, M., and Schlichting, I. (1998) Structural basis for efficient phosphorylation of 3'-azidothymidine monophosphate by Escherichia coli thymidylate kinase. *Proc. Natl. Acad. Sci. U. S. A.* 95, 14045–14050.
- (22) Whittingham, J. L., Carrero-Lerida, J., Brannigan, J. A., Ruiz-Perez, L. M., Silva, A. P., Fogg, M. J., Wilkinson, A. J., Gilbert, I. H., Wilson, K. S., and Gonzalez-Pacanowska, D. (2010) Structural basis for the efficient phosphorylation of AZT-MP (3'-azido-3'-deoxythymidine monophosphate) and dGMP by Plasmodium falciparum type I thymidylate kinase. *Biochem. J.* 428, 499–509.
- (23) Su, J. Y., and Sclafani, R. A. (1991) Molecular cloning and expression of the human deoxythymidylate kinase gene in yeast. *Nucleic Acids Res.* 19, 823–827.
- (24) Lee, L. S., and Cheng, Y. (1977) Human thymidylate kinase. Purification, characterization, and kinetic behavior of the thymidylate kinase derived from chronic myelocytic leukemia. *J. Biol. Chem.* 252, 5686–5691.
- (25) Cauda, R. (2009) Candidaemia in patients with an inserted medical device. *Drugs* 69 (Suppl. 1), 33–38.
- (26) Coleman, D. C., Moran, G. P., McManus, B. A., and Sullivan, D. J. (2010) Mechanisms of antifungal drug resistance in Candida dubliniensis. *Future Microbiol.* 5, 935–949.
- (27) Ann Chai, L. Y., Denning, D. W., and Warn, P. (2010) Candida tropicalis in human disease. *Crit. Rev. Microbiol.* 36, 282–298.
- (28) Martin, M. V. (1999) The use of fluconazole and itraconazole in the treatment of Candida albicans infections: a review. *J. Antimicrob. Chemother.* 44, 429–437.
- (29) Morschhauser, J. (2016) The development of fluconazole resistance in Candida albicans - an example of microevolution of a fungal pathogen. *J. Microbiol. (Seoul, Repub. Korea)* 54, 192–201.
- (30) Dereeper, A., Guignon, V., Blanc, G., Audic, S., Buffet, S., Chevenet, F., Dufayard, J. F., Guindon, S., Lefort, V., Lescot, M., Claverie, J. M., and Gascuel, O. (2008) Phylogeny.fr: robust phylogenetic analysis for the non-specialist. *Nucleic Acids Res.* 36, W465–469.
- (31) Blondin, C., Serina, L., Wiesmuller, L., Gilles, A. M., and Barzu, O. (1994) Improved spectrophotometric assay of nucleoside monophosphate kinase activity using the pyruvate kinase/lactate dehydrogenase coupling system. *Anal. Biochem.* 220, 219–221.
- (32) Bujacz, G., Wrzesniewska, B., and Bujacz, A. (2010) Cryoprotection properties of salts of organic acids: a case study for a tetragonal crystal of HEW lysozyme. *Acta Crystallogr., Sect. D: Biol. Crystallogr.* 66, 789–796.
- (33) Winn, M. D., Ballard, C. C., Cowtan, K. D., Dodson, E. J., Emsley, P., Evans, P. R., Keegan, R. M., Krissinel, E. B., Leslie, A. G. W., McCoy, A., McNicholas, S. J., Murshudov, G. N., Pannu, N. S., Potterton, E. A., Powell, H. R., Read, R. J., Vagin, A., and Wilson, K. S. (2011) Overview of the CCP4 suite and current developments. *Acta Crystallogr., Sect. D: Biol. Crystallogr.* 67, 235–242.
- (34) Batty, T. G., Kontogiannis, L., Johnson, O., Powell, H. R., and Leslie, A. G. (2011) iMOSFLM: a new graphical interface for diffraction-image processing with MOSFLM. *Acta Crystallogr., Sect. D: Biol. Crystallogr.* 67, 271–281.
- (35) Evans, P. R., and Murshudov, G. N. (2013) How good are my data and what is the resolution? *Acta Crystallogr., Sect. D: Biol. Crystallogr.* 69, 1204–1214.
- (36) Stein, N. (2008) CHAINSAW: a program for mutating pdb files used as templates in molecular replacement. *J. Appl. Crystallogr.* 41, 641–643.
- (37) Lavie, A., Konrad, M., Brundiers, R., Goody, R. S., Schlichting, I., and Reinstein, J. (1998) Crystal structure of yeast thymidylate kinase complexed with the bisubstrate inhibitor P1-(5'-adenosyl) P5-(5'-thymidyl) pentaphosphate (TPSA) at 2.0 Å resolution: implications for catalysis and AZT activation. *Biochemistry* 37, 3677–3686.
- (38) McCoy, A. J., Grosse-Kunstleve, R. W., Adams, P. D., Winn, M. D., Storoni, L. C., and Read, R. J. (2007) Phaser crystallographic software. *J. Appl. Crystallogr.* 40, 658–674.
- (39) Vagin, A. A., Steiner, R. A., Lebedev, A. A., Potterton, L., McNicholas, S., Long, F., and Murshudov, G. N. (2004) REFMAC 5 dictionary: organization of prior chemical knowledge and guidelines for its use. *Acta Crystallogr., Sect. D: Biol. Crystallogr.* 60, 2184–2195.
- (40) Emsley, P., Lohkamp, B., Scott, W. G., and Cowtan, K. (2010) Features and development of Coot. *Acta Crystallogr., Sect. D: Biol. Crystallogr.* 66, 486–501.

- (41) Joosten, R. P., Long, F., Murshudov, G. N., and Perrakis, A. (2014) The PDB_REDO server for macromolecular structure model optimization. *IUCr* *1*, 213–220.
- (42) Topalis, D., Collinet, B., Gasse, C., Dugue, L., Balzarini, J., Pochet, S., and Deville-Bonne, D. (2005) Substrate specificity of vaccinia virus thymidylate kinase. *FEBS J.* *272*, 6254–6265.
- (43) Studier, F. W. (2005) Protein production by auto-induction in high density shaking cultures. *Protein Expression Purif.* *41*, 207–234.
- (44) Goto, N. K., and Kay, L. E. (2000) New developments in isotope labeling strategies for protein solution NMR spectroscopy. *Curr. Opin. Struct. Biol.* *10*, 585–592.
- (45) Sinha, K., Sangani, S. S., Kehr, A. D., Rule, G. S., and Jen-Jacobson, L. (2016) Metal Ion Binding at the Catalytic Site Induces Widely Distributed Changes in a Sequence Specific Protein-DNA Complex. *Biochemistry* *55*, 6115–6132.
- (46) Phillips, J. C., Braun, R., Wang, W., Gumbart, J., Tajkhorshid, E., Villa, E., Chipot, C., Skeel, R. D., Kalé, L., and Schulten, K. (2005) Scalable molecular dynamics with NAMD. *J. Comput. Chem.* *26*, 1781–1802.
- (47) Ostermann, N., Segura-Pena, D., Meier, C., Veit, T., Monnerjahn, C., Konrad, M., and Lavie, A. (2003) Structures of human thymidylate kinase in complex with prodrugs: implications for the structure-based design of novel compounds. *Biochemistry* *42*, 2568–2577.
- (48) Ostermann, N., Lavie, A., Padiyar, S., Brundiers, R., Veit, T., Reinstein, J., Goody, R. S., Konrad, M., and Schlichting, I. (2000) Potentiating AZT activation: structures of wild-type and mutant human thymidylate kinase suggest reasons for the mutants' improved kinetics with the HIV prodrug metabolite AZTMP. *J. Mol. Biol.* *304*, 43–53.
- (49) Kandeel, M., Ando, T., Kitamura, Y., Abdel-Aziz, M., and Kitade, Y. (2009) Mutational, inhibitory and microcalorimetric analyses of Plasmodium falciparum TMP kinase. Implications for drug discovery. *Parasitology* *136*, 11–25.
- (50) Caillat, C., Topalis, D., Agrofoglio, L. A., Pochet, S., Balzarini, J., Deville-Bonne, D., and Meyer, P. (2008) Crystal structure of poxvirus thymidylate kinase: an unexpected dimerization has implications for antiviral therapy. *Proc. Natl. Acad. Sci. U. S. A.* *105*, 16900–16905.